frontiers in Chemistry

ORIGINAL RESEARCH
published: 23 July 2019
doi: 10.3389/fchem.2019.00521

Highly Ordered Mesoporous $NiCo_2O_4$ as a High Performance Anode Material for Li-Ion Batteries

Qilong Ren[1†], Guangyu Wu[2†], Weinan Xing[2*], Jiangang Han[2], Pingping Li[2], Bo Li[3*], Junye Cheng[4], Shuilin Wu[4], Rujia Zou[1] and Junqing Hu[1*]*

[1] State Key Laboratory for Modification of Chemical Fibers and Polymer Materials, College of Materials Science and Engineering, Donghua University, Shanghai, China, [2] College of Biology and the Environment, Nanjing Forestry University, Nanjing, China, [3] Department of Vascular Surgery, Shanghai Ninth People's Hospital, Shanghai JiaoTong University School of Medicine, Shanghai, China, [4] Center of Super-Diamond and Advanced Films, Department of Materials Science and Engineering, City University of Hong Kong, Hong Kong, China

OPEN ACCESS

Edited by:
Min Zeng,
Lanzhou Institute of Chemical Physics (CAS), China

Reviewed by:
Hui Yang,
Jiangxi University of Science and Technology, China
Ming Ma,
Shanghai Institute of Ceramics (CAS), China

***Correspondence:**
Guangyu Wu
gywuchem@163.com
Weinan Xing
xingweinan@126.com
Bo Li
boli@shsmu.edu.cn
Junqing Hu
hu.junqing@dhu.edu.cn

[†] *These authors have contributed equally to this work*

Specialty section:
This article was submitted to Electrochemistry, a section of the journal Frontiers in Chemistry

Received: *20 June 2019*
Accepted: *08 July 2019*
Published: *23 July 2019*

Citation:
Ren Q, Wu G, Xing W, Han J, Li P, Li B, Cheng J, Wu S, Zou R and Hu J (2019) Highly Ordered Mesoporous $NiCo_2O_4$ as a High Performance Anode Material for Li-Ion Batteries. Front. Chem. 7:521. doi: 10.3389/fchem.2019.00521

The controlled synthesis of highly ordered mesoporous structure has attracted considerable attention in the field of electrochemistry because of its high specific surface area which can contribute the transportation of ions. Herein, a general nano-casting approach is proposed for synthesizing highly ordered mesoporous $NiCo_2O_4$ microspheres. The as-synthesized mesoporous $NiCo_2O_4$ microsphere materials with high Brunner-Emmett-Teller (BET) surface area (~97.77 m^2g^{-1}) and uniform pore size distribution around 4 nm exhibited a high initial discharge capacity of ~1,467 $mAhg^{-1}$, a good rate capability as well as cycling stability. The superior electrochemical performance was mainly because of the highly porous nature of $NiCo_2O_4$, which rendered volume expansion during the process of cycling and shortened lithium-ions transport pathways. These properties showcase the inherent potential for use of highly ordered mesoporous $NiCo_2O_4$ microspheres as a potential anode material for lithium-ion batteries in the future.

Keywords: highly ordered, mesoporous, $NiCo_2O_4$, lithium-ion batteries, nano-casting

INTRODUCTION

Lithium-ion batteries (Yoo et al., 2008; Pan et al., 2013) have been proven to be viable alternatives to traditional energy storage devices and are vital tools when coupled with emerging renewable energy sources (Lewis and Nocera, 2006; Song, 2006; Chheda et al., 2007) (i.e., wind, solar, *etc.*). However, current energy demands outpace what is commercial systems are capable of, leading to the development of next-generation lithium-ion batteries (Liu et al., 2012; Lu et al., 2018; Shen et al., 2018). Particularly, the electrode is vital for optimal electrochemical performance (Toupin et al., 2004; Jiang et al., 2012; Wang et al., 2012; Yang et al., 2019a); however, conventional anode materials (Courtel et al., 2011; Chen et al., 2013; Chang et al., 2014) such as graphite have low theoretical specific capacities (372 mAh g^{-1}) and fail to satisfy energy storage demands. Consequently, transition metal oxides (TMOs) (Yuan et al., 2014; Tabassum et al., 2018) have been proposed as viable alternatives, attributed to high energy densities, which result in capacities more than double of those observed with graphite. However, this capacity relies on the morphology and structure of the TMO, which can suffer from undesired volume expansion and collapse of the structure as the battery cycles, leading to catastrophic failure.

Recently, space designed nanostructures have been acknowledged as an effective strategy to remit the volume expansion as well as shorten the lithium-ion transport pathways by providing a larger specific surface area, including implementation of a porous network (Wen et al., 2007; Lou et al., 2008; Shen et al., 2012, 2014; Yuan et al., 2012; Qie et al., 2013; Yang et al., 2019b), mesopores structures. For example, mesoporous Co_3O_4 (Li et al., 2008), NiO (Yin et al., 2018), $NiCo_2O_4$ (Li et al., 2018), and SnO_2 (Han et al., 2019) have been fabricated and have shown good electrochemical performance. However, limited attention has been focused to study ternary systems such as $NiCo_2O_4$ despite a higher electrical conductivity and specific capacity owing to its enhanced chemical kinetics. Inspired by ammonium hydrogen carbonate-assisted solvothermal route to prepare $Ni_{0.33}Co_{0.67}CO_3$ microspheres (Li et al., 2013), they led to a recent breakthrough technique to form mesoporous microspheres, we present a modified structure design containing ordered mesopores to further improve the electrochemical performance of $NiCo_2O_4$.

Herein, we developed a template-assisted method to synthesize novel $NiCo_2O_4$ microspheres containing highly ordered mesoporous structures and nanoparticles to effectively alleviate the huge volume expansion and enhance the electrical conductivity. The synthesis process is schematically shown in **Figure 1**. Firstly, mesoporous silica (KIT-6) is synthesized as a template by a typical approach which is illustrated in the experiment section in detail. Then the template is immersed in the mixed solution of $Ni(NO_3)_2$ and $Co(NO_3)_2$ to introduce the Ni^{2+} and Co^{2+} to be filled into KIT-6. After a subsequent calcination step at 450°C under N_2 atmosphere, the $NiCo_2O_4$@KIT-6 is successfully prepared. Finally, NaOH solution is utilized to remove the template of KIT-6 in the $NiCo_2O_4$@KIT-6 and obtain mesoporous $NiCo_2O_4$ microspheres. When acted as an anode material for Li-ion batteries, mesoporous $NiCo_2O_4$ microsphere electrode exhibits the superior electrochemical performance, whose stable specific capacity was 430 $mAhg^{-1}$ after 100 cycles, which is better than that of the non-porous $NiCo_2O_4$ (270 $mAhg^{-1}$ after 100 cycles). The improved lithium storage performance mainly benefits from the rationally designed mesoporous structures of $NiCo_2O_4$. We believe that this versatile strategy could be extended to more ternary TMO materials for the development of high property electrode in LIBs.

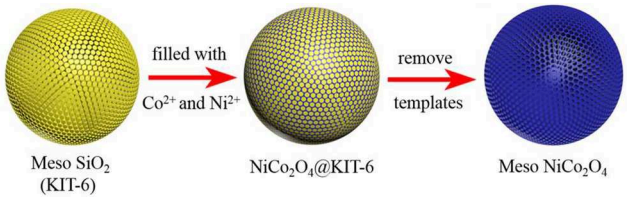

FIGURE 1 | Schematic illustration of the preparation for mesoporous $NiCo_2O_4$ microspheres.

EXPERIMENTAL SECTION

Materials

All chemicals (analytical reagent grade) used in this work, including polyethylene oxide-polypropylene oxide-polyethylene oxide (PEO-PPO-PEO, P123, MW = 5.8 K), hydrochloric acid, n-butanol, tetraethyl orthosilicate (TEOS), $Co(NO_3)_2{\bullet}6H_2O$, $Ni(NO_3)_2{\bullet}6H_2O$ and ethanol were purchased from Sigma-Aldrich.

Material Synthesis

Synthesis of Mesoporous SiO_2 (KIT-6)

The typical synthetic process was as follows (Zhou et al., 2018): 4.75 g of P123 were dissolved in a mixed solution containing 163 mL of deionized (DI) water and 7.5 ml of concentrated hydrochloric acid under stirring at 35°C. Once the P123 was fully dissolved, 4.53 g of n-butanol were added. After 1 h, TEOS (9.675 g) were added into the above mixed solution. The solution was then stirred for an additional 24 h at 35°C, followed by another 24 h incubation at 35°C. Cooling the mixed solution to room temperature, the precipitates could be collected by centrifugation for 3 times and moved to a vacuum oven at 90°C for 12 h. Then, after calcining the collected deposit at 550°C for 6 h, white mesoporous SiO_2 was obtained.

Synthesis of Mesoporous $NiCo_2O_4$ Microspheres

In a simple process, 0.4 g of KIT-6 were added to a solution containing 4 ml of 1 M $Co(NO_3)_2{\cdot}6H_2O$ and 2 ml of 1 M $Ni(NO_3)_2{\cdot}6H_2O$ in ethanol under stirring for 1.5 h at room temperature. Then, the solution was heated at 70°C until the ethanol was completely evaporated, and the solid was calcined at 200°C for 4 h. Immediately following, 2 mL of 1 M $Co(NO_3)_2{\cdot}6H_2O$ and 1 mL of $Ni(NO_3)_2{\cdot}6H_2O$ in ethanol were added following the previous steps and an additional calcination 450°C for 6 h. To obtain mesoporous $NiCo_2O_4$ microspheres, the powder was immersed in a 2 M NaOH solution to etch away the KIT-6 templates. Then, the samples were collected by centrifugation, washed for 3 times and moved to a vacuum oven at 60°C for 12 h. As a control, conventional $NiCo_2O_4$ microspheres were produced through the above-mentioned process without KIT-6 templates.

Materials Characterization

The mesoporous $NiCo_2O_4$ microspheres were characterized by using a PANalytical X' Pert X-ray diffractometer (Holland), with Cu-Kα radiation at 40 kV and 40 mA, selected-area electron diffraction (SAED), scanning electron microscope (SEM, S-4800) and transmission electron microscope (TEM, JEM-2100F). The N_2 adsorption/desorption isotherms were used to calculate the specific surface area and Barrett-Joyner-Halenda (BJH) equation was used to calculate the pore size distribution and average pore diameter.

RESULTS AND DISCUSSION

The mesoporous $NiCo_2O_4$ microspheres were prepared via nano-casting, with the crystalline structure and phase purity

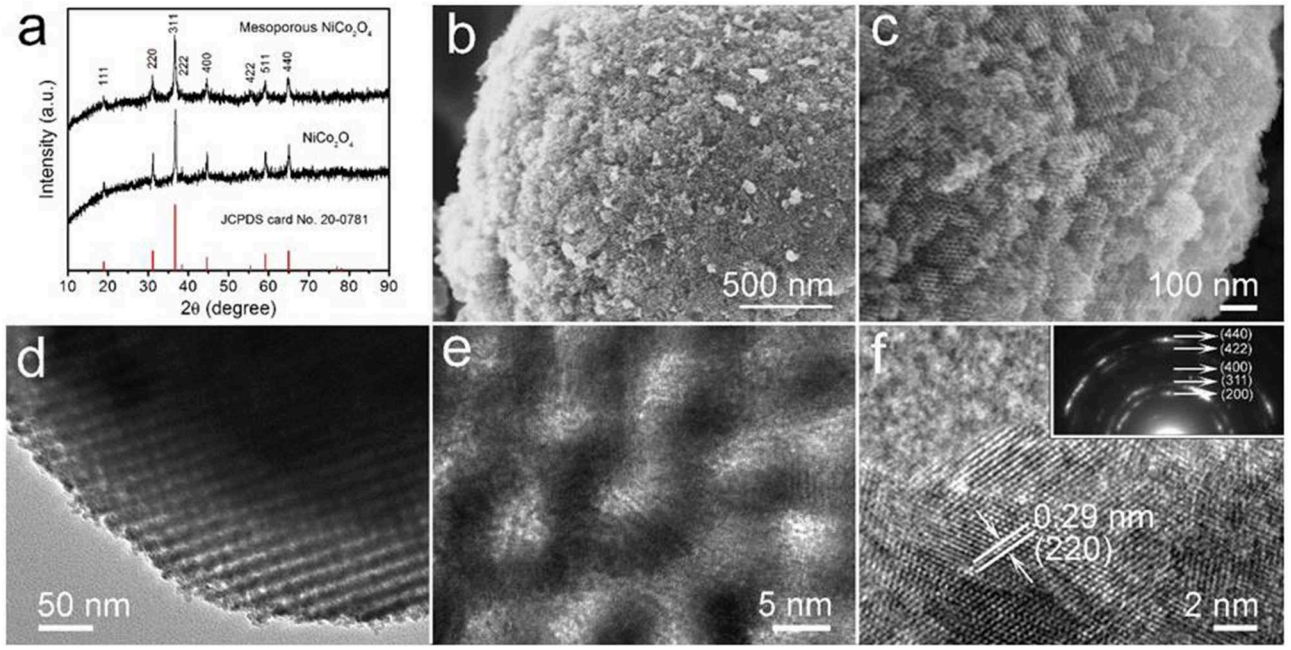

FIGURE 2 | (a) XRD patterns of mesoporous and non-porous $NiCo_2O_4$. **(b,c)** high magnification SEM images of mesoporous $NiCo_2O_4$. **(d)** TEM image and **(e,f)** high-resolution TEM image of mesoporous $NiCo_2O_4$. Inset in **(f)** shows the corresponding SAED pattern.

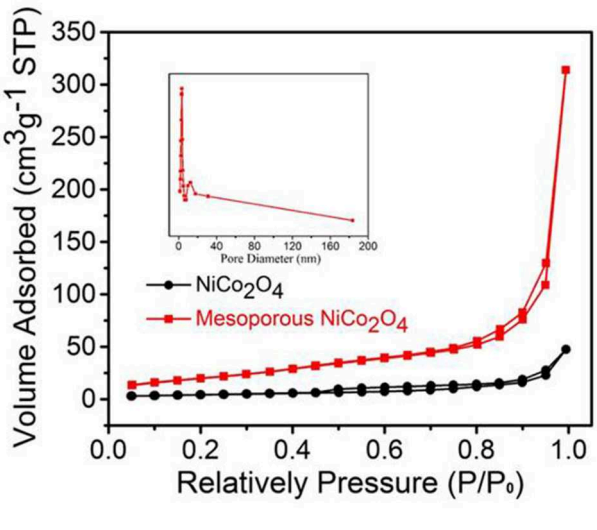

FIGURE 3 | Nitrogen adsorption-desorption isotherm and the corresponding pore size distribution of ordinary $NiCo_2O_4$ and mesoporous $NiCo_2O_4$.

characterized by X-ray diffraction (XRD). **Figure 2a** compares the diffraction patterns of both mesoporous and non-porous $NiCo_2O_4$ microspheres, showing eight obvious peaks at 2θ values of 18.9, 31.1, 36.7, 38.4, 44.6, 55.4, 59.1, and 64.9 for the (111), (220), (311), (222), (400), (422), (511), and (440) planes, respectively, which consist with the cubic spinel $NiCo_2O_4$ (JCPDS No.20-0781)without any apparent impurities.

The morphology and structure of obtained $NiCo_2O_4$are elucidated by SEM and TEM, as shown in **Figures 2b,c**, the surface morphology of the mesoporous microspheres, when compared to nonporous structures (**Figure S1**), is significantly rougher with highly ordered, uniform pores. This suggests that the polymeric precursor was fully injected within the KIT-6 microspheres, allowing the continuity of the mesoporous structure in subsequent deposition reactions. The highly ordered pores of the $NiCo_2O_4$ microspheres are clearly revealed with a pore size of ∼4 nm as shown by high-resolution TEM in **Figures 2d,e**. Additionally, in **Figure 2f**, the measured interplanar distance was found to be 0.29 nm, which aligns well with the (220) planes of spinel $NiCo_2O_4$. It is worth noting that well-defined diffraction rings were presented by the SAED pattern (Inset in **Figure 2f**), which correspond to the (440), (422), (400), (311), and (200) planes. The polycrystalline diffraction rings are in accordance with the result from the XRD pattern.

The pore diameter distribution and specific surface area of mesoporous $NiCo_2O_4$ samples were determined via N_2 adsorption-desorption measurements. The result of specific surface area was calculated from the isotherms (**Figure 3**) was 97.77 m^2g^{-1} for mesoporous $NiCo_2O_4$ microspheres, while the non-porous $NiCo_2O_4$ microspheres were 26.63 m^2g^{-1}. Additionally, the mesoporous structure was further analyzed by pore diameter distribution in the inset of **Figure 3**. $NiCo_2O_4$ microspheres displayed a pore volume (0.494 cm^3g^{-1}) with an average pore diameter of 3.416 nm. Ascribed to this special microsphere structure, the mesoporous structure could shorten the diffusion paths for lithium ions and provided buffering space to adapt

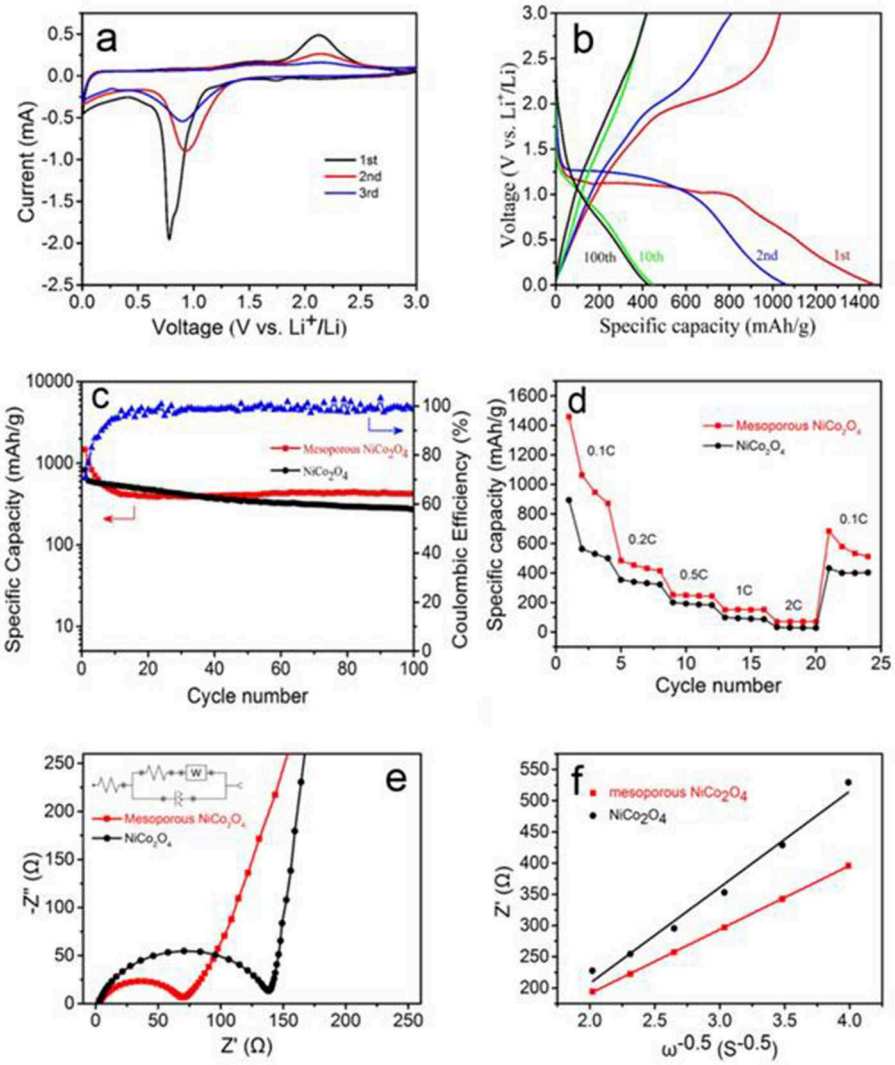

FIGURE 4 | First three consecutive CV curves of mesoporous $NiCo_2O_4$ **(a)**, galvanostatic discharge and charge profiles for 1st, 2nd,10th, 100th cycles of mesoporous $NiCo_2O_4$ **(b)** at the current densities of 100 mA.g^{-1}, cycling performance of ordinary $NiCo_2O_4$ and mesoporous $NiCo_2O_4$ at the current densities of 100 mAh.g^{-1} **(c)**, rate performances for ordinary $NiCo_2O_4$ and mesoporous $NiCo_2O_4$ at various current densities **(d)**. EIS pattern of ordinary $NiCo_2O_4$ and mesoporous $NiCo_2O_4$ **(e)**. The typical plots for Z' vs. $\omega^{-0.5}$ for the mesoporous $NiCo_2O_4$ **(f)**.

the volume expansion during the process of Li^+ insertion and extraction.

To confirm whether the mesoporous $NiCo_2O_4$ microspheres would be applicable as the anode materials in lithium-ion batteries, the as-prepared products were further investigated using cyclic voltammetry (CV), where **Figure 4a** exhibits the first three cycles of the mesoporous $NiCo_2O_4$ microspheres. In the 1st cycle, one dominant peak at 0.8 V could be assigned to the decomposition and reduction of Ni and Co ions. Meanwhile, the anodic peaks at approximately 2.1 V could be owing to the oxidation reaction of metallic Ni and Co to NiO and CoO. In subsequent tests, the cathodic peak broadened and shifted to 1.0 V. According to the analysis of the CV curves and previous literature reports, the Li reactions for mesoporous $NiCo_2O_4$ materials are as follows:

$$NiCo_2O_4 + 8Li^+ + 8e^- = Ni + 2Co + 4Li_2O \quad (1)$$

$$Ni + Li_2O = NiO + 2Li^+ + 2e^- \quad (2)$$

$$2Co + 2Li_2O = 2CoO + 4Li^+ + 4e^- \quad (3)$$

$$2CoO + 2/3Li_2O = 2/3Co_3O_4 + 4/3Li^+ + 4/3e^- \quad (4)$$

Galvanostatic tests were executed to ensure the influence of highly ordered mesoporous $NiCo_2O_4$ samples on the specific capacity values and capacity retention. The 1st, 2nd, 10th, and 100th cycles of the galvanostatic charge and discharge curves for mesoporous samples, at a current of 100 mA.g^{-1}, are shown

in **Figure 4b**. A long voltage plateau was showed in the initial discharge curve between 0.7 and 1.2 V, corresponding to the strong reduction peak that appeared during the first cathodic CV scan. The initial charge capacity for the mesoporous $NiCo_2O_4$ microspheres was ∼1467 $mAhg^{-1}$, which is markedly higher than the non-porous $NiCo_2O_4$ microspheres (∼820 $mAhg^{-1}$, **Figure S2**); however, this decreased to 1,060 $mAhg^{-1}$ after the 2nd discharge. The irreversible capacity increase during the 1st charge may be due to the generation of a solid electrolyte interface (SEI) layer.

A comparison of the specific capacity values obtained for non-porous $NiCo_2O_4$ and mesoporous $NiCo_2O_4$ over 100 cycles plotted is shown in **Figure 4c**. The non-porous $NiCo_2O_4$ suffers the most severe capacity fading with capacity values decreasing to 270 $mAhg^{-1}$ after 100 cycles, while the capacity retention was improved for mesoporous $NiCo_2O_4$ microspheres, obtaining capacity values of 430 $mAhg^{-1}$ after 100 cycles. The significant increase in the capacities for mesoporous $NiCo_2O_4$ compared to ordinary $NiCo_2O_4$ is attributed to the inherent properties of the mesoporous structure. Nevertheless, the final capacity is relatively low compared to the initial capacity, which may be attributed to the aperture being too small to relieve the expansion of the active material completely (Bhaway et al., 2017). For conversion-mode materials, the mesoporous $NiCo_2O_4$ provides particularly high buffering space, to adapt the large volume expansion during the process of Li^+ insertion/extraction and shorten the diffusion paths for lithium ions due to the interconnected architectures (**Figure S3**). Moreover, the coulombic efficiency for mesoporous $NiCo_2O_4$ over 100 cycles is also shown in **Figure 4c**. The initial coulombic efficiency is quite low (∼70%); however, the efficiency remains >95% after the 10th cycle. The rate performance of ordinary $NiCo_2O_4$ microspheres and mesoporous $NiCo_2O_4$ microspheres at various current densities were then compared in **Figure 4d**. The mesoporous $NiCo_2O_4$ microsphere electrode exhibits high initial discharge capacity and the capacity was recession with the increase of current density. However, the mesoporous $NiCo_2O_4$ microsphere electrode exhibited a higher capacity and rate of lithium-ion storage than the non-porous $NiCo_2O_4$ microsphere electrode.

To further investigate the mechanism for the improved electrochemical performance of the mesoporous $NiCo_2O_4$ microsphere, electrochemical impedance measurements (**Figure 4e**) and a fitting process (**Figure S4**) were measured containing the mesoporous $NiCo_2O_4$ electrode and ordinary $NiCo_2O_4$. As shown in **Figure 4e**, a semicircle and a straight line were acquired in the high frequency part and low frequency part, respectively. The intersection point from the curve in the high frequency part is on behalf of the electrolyte resistance. Moreover, the high frequency semicircle corresponds to the charge transfer resistance and the low frequency region with an inclined line represents the process of Li-ion diffusion. The initial value for charge transfer resistance is 66 Ω, which is far less than the ordinary $NiCo_2O_4$ (134 Ω, **Table S1**), which could be related to the more effective ion and electron transfer in the interface of electrolyte and active material, so that the cell has improved electrode reaction kinetics and a better cell cycling results.

TABLE 1 | Warburg factor (σ) and diffusion coefficient (D_{Li}^+) of sample ordinary $NiCo_2O_4$ and mesoporous $NiCo_2O_4$.

Materials	σ(Ω $s^{-0.5}$)	D_{Li}^+ (cm^2s^{-1})
Ordinary $NiCo_2O_4$	153.78	1.64×10^{-12}
Mesoporous $NiCo_2O_4$	102.48	2.46×10^{-12}

Moreover, the diffusion coefficient of the lithium ions (D_{Li}^+) can be confirmed in accordance with the following equation:

$$D_{Li^+} = \frac{0.5R^2T^2}{A^2F^4c^2\sigma_\omega^2}$$

Where R = gas constant, T = absolute temperature, A = surface area of the electrode, F = Faraday constant, c = concentration of Li+ in the material, and σ = Warburg factor obeying the following relationship:

$$Z_{Re} = R_S + R_{ct} + \sigma\omega^{-0.5}$$

Where Z_{Re} is the real part of impedance, thus ω is the angular frequency at low frequency. The linear relationship of Z_{Re} and $\omega^{-0.5}$ is shown in **Figure 4f**, with the slope of the fitted straight line indicating the value of σ. **Table 1** revealed the calculated values of σ and D_{Li}^+, where it can be clearly seen that the mesoporous $NiCo_2O_4$ exhibits a higher value of D_{Li}^+ than nonporous $NiCo_2O_4$.

CONCLUSION

Highly ordered mesoporous $NiCo_2O_4$ microspheres with a honeycomb-like structure, were synthesized via a nano-casting method. The mesoporous $NiCo_2O_4$ electrode possesses a high initial discharge capacity of ∼1,467 $mAh.g^{-1}$ at 100 mAg^{-1} and it exhibited both a high surface area and good rate capability. Such high electrochemical performance is due to its excellent surface area of mesoporous $NiCo_2O_4$ and the rapid ion transport in the electrolyte/electrode interface. This work may open a new sight in the synthesis of excellent Li-storage electrode materials and show an application in a promising candidate for Li-ion batteries.

DATA AVAILABILITY

The raw data supporting the conclusions of this manuscript will be made available by the authors, without undue reservation, to any qualified researcher. Requests to access the datasets should be directed to hu.junqing@dhu.edu.cn.

AUTHOR CONTRIBUTIONS

GW, BL, and JHu designed the project. QR, WX, JHa, PL, JC, SW, and RZ carried out the experiment and performed the experimental data analysis. QR, GW, and WX wrote the paper. BL revised the manuscript. All authors contributed to discussion of the results.

FUNDING

This work was financially supported by the National Key Research and Development of China (2017YFC0505803), the National Natural Science Foundation of China (41471191), Qing Lan Project of Jiangsu Province (Qinglan2016-15), Priority Academic Program Development of Jiangsu Higher Education Institutions (PAPD), and the Fundamental Research Funds for the Central Universities (grant no. CUSF-DH-D-2017044).

SUPPLEMENTARY MATERIAL

The Supplementary Material for this article can be found online at: https://www.frontiersin.org/articles/10.3389/fchem.2019.00521/full#supplementary-material

REFERENCES

Bhaway, S. M., Qiang, Z., Xia, Y., Xia, X., Lee, B., Yager, K. G., et al. (2017). Operando grazing incidence small-angle X-ray scattering/X-ray diffraction of model ordered mesoporous lithium-ion battery anodes. *ACS Nano* 11, 1443–1454. doi: 10.1021/acsnano.6b06708

Chang, J., Huang, X., Zhou, G., Cui, S., Hallac, P. B., Jiang, J., et al. (2014). Multilayered Si nanoparticle/reduced graphene oxide hybrid as a high-performance lithium-ion battery anode. *Adv. Mater.* 26, 758–764. doi: 10.1002/adma.201302757

Chen, Z., Belharouak, I., Sun, Y. K., and Amine, K. (2013). Titanium-based anode materials for safe lithium-ion batteries. *Adv. Funct. Mater.* 23, 959–969. doi: 10.1002/adfm.201200698

Chheda, J. N., Huber, G. W., and Dumesic, J. A. (2007). Liquid-phase catalytic processing of biomass-derived oxygenated hydrocarbons to fuels and chemicals. *Angew. Chem. Int. Ed.* 46, 7164–7183. doi: 10.1002/anie.200604274

Courtel, F. M., Duncan, H., Abu-Lebdeh, Y., and Davidson, I. J. (2011). High capacity anode materials for Li-ion batteries based on spinel metal oxides AMn_2O_4 (A = Co, Ni, and Zn). *J. Mater. Chem.* 21, 10206–10218. doi: 10.1039/C0JM04465B

Han, N., Wang, Y., Deng, J., Zhou, J., Wu, Y., Yang, H., et al. (2019). Self-templated synthesis of hierarchical mesoporous SnO_2 nanosheets for selective CO_2 reduction. *J. Mater. Chem. A* 7, 1267–1272. doi: 10.1039/C8TA10959A

Jiang, J., Li, Y., Liu, J., Huang, X., Yuan, C., and Lou, X. W. (2012). Recent advances in metal oxide-based electrode architecture design for electrochemical energy storage. *Adv. Mater.* 24, 5166–5180. doi: 10.1002/adma.201202146

Lewis, N. S., and Nocera, D. G. (2006). Powering the planet: chemical challenges in solar energy utilization. *Proc. Natl. Acad. Sci. U. S. A.* 103, 15729–15735. doi: 10.1073/pnas.0603395103

Li, J., Xiong, S., Liu, Y., Ju, Z., and Qian, Y. (2013). High electrochemical performance of monodisperse $NiCo_2O_4$ mesoporous microspheres as an anode material for li-ion batteries. *ACS Appl. Mater. Interfaces* 5, 981–988. doi: 10.1021/am3026294

Li, W., Zhang, B., Lin, R., Ho-Kimura, S., He, G., and Zhou, X., et al (2018). A dendritic nickel cobalt sulfide nanostructure for alkaline battery electrodes. *Adv. Funct. Mater.* 28:1705937. doi: 10.1002/adfm.201705937

Li, Y., Tan, B., and Wu, Y. (2008). Mesoporous Co_3O_4 nanowire arrays for lithium ion batteries with high capacity and rate capability. *Nano Lett.* 8, 265–270. doi: 10.1021/nl0725906

Liu, N., Wu, H., McDowell, M. T., Yao, Y., Wang, C., and Cui, Y. (2012). A yolk-shell design for stabilized and scalable li-ion battery alloy anodes. *Nano Lett.* 12, 3315–3321. doi: 10.1021/nl3014814

Lou, X. W., Deng, D., Lee, J. Y., and Archer, L. A. (2008). Thermal formation of mesoporous single-crystal Co3O4 nano-needles and their lithium storage properties. *J. Mater. Chem.* 18, 4397–4401. doi: 10.1039/B810093D

Lu, Y., Yu, L., and Lou, X. W. (2018). Nanostructured conversion-type anode materials for advanced lithium-ion batteries. *Chem* 4, 972–996. doi: 10.1016/j.chempr.2018.01.003

Pan, H., Hu, Y.-S., and Chen, L. (2013). Room-temperature stationary sodium-ion batteries for large-scale electric energy storage. *Energy Environ. Sci.* 6, 2338–2360. doi: 10.1039/C3EE40847G

Qie, L., Chen, W., Xu, H., Xiong, X., Jiang, Y., Zou, F., et al. (2013). Synthesis of functionalized 3D hierarchical porous carbon for high-performance supercapacitors. *Energy Environ. Sci.* 6, 2497–2504. doi: 10.1039/C3EE41638K

Shen, L., Che, Q., Li, H., and Zhang, X. (2014). Mesoporous $NiCo_2O_4$ nanowire arrays grown on carbon textiles as binder-free flexible electrodes for energy storage. *Adv. Funct. Mater.* 24, 2630–2637. doi: 10.1002/adfm.201303138

Shen, L., Zhang, X., Uchaker, E., Yuan, C., and Cao, G. (2012). $Li_4Ti_5O_{12}$ nanoparticles embedded in a mesoporous carbon matrix as a superior anode material for high rate lithium ion batteries. *Adv. Energy Mater.* 2, 691–698. doi: 10.1002/aenm.201100720

Shen, X., Liu, H., Cheng, X. B., Yan, C., and Huang, J. Q. (2018). Beyond lithium ion batteries: higher energy density battery systems based on lithium metal anodes. *Energy Storage Mater.* 12, 161–175. doi: 10.1016/j.ensm.2017.12.002

Song, C. (2006). Global challenges and strategies for control, conversion and utilization of CO_2 for sustainable development involving energy, catalysis, adsorption and chemical processing. *Catalysis Today* 115, 2–32. doi: 10.1016/j.cattod.2006.02.029

Tabassum, H., Zou, R., Mahmood, A., Liang, Z., Wang, Q., Zhang, H., et al. (2018). A universal strategy for hollow metal oxide nanoparticles encapsulated into B/N co-doped graphitic nanotubes as high-performance lithium-ion battery anodes. *Adv. Mater.* 30:1705441. doi: 10.1002/adma.201705441

Toupin, M., Brousse, T., and Bélanger, D. (2004). Charge storage mechanism of MnO_2 electrode used in aqueous electrochemical capacitor. *Chem. Mater.* 16, 3184–3190. doi: 10.1021/cm049649j

Wang, G., Zhang, L., and Zhang, J. (2012). A review of electrode materials for electrochemical supercapacitors. *Chem. Soc. Rev.* 41, 797–828. doi: 10.1039/C1CS15060J

Wen, Z., Wang, Q., Zhang, Q., and Li, J. (2007). *In situ* growth of mesoporous SnO_2 on multiwalled carbon nanotubes: a novel composite with porous-tube structure as anode for lithium batteries. *Adv. Funct. Mater.* 17, 2772–2778. doi: 10.1002/adfm.200600739

Yang, H., Ye, S., Wang, Y., Zhou, J., Jia, J., Chen, J., et al. (2019a). Scalable production of hierarchical n-doping porous carbon@cu composite fiber based on rapid gelling strategy for high-performance supercapacitor. *J. Alloys Compd.* 792, 976–982. doi: 10.1016/j.jallcom.2019.04.138

Yang, H., Ye, S., Zhou, J., and Liang, T. (2019b). Biomass-derived porous carbon materials for supercapacitor. *Front. Chem.* 7:274. doi: 10.3389/fchem.2019.00274

Yin, X., Chen, H., Zhi, C., Sun, W., Lv, L.-P., and Wang, Y. (2018). Functionalized graphene quantum dot modification of yolk-shell NiO microspheres for superior lithium storage. *Small* 14:1800589. doi: 10.1002/smll.201800589

Yoo, E., Kim, J., Hosono, E., Zhou, H.-S., Kudo, T., and Honma, I. (2008). Large Reversible Li storage of graphene nanosheet families for use in rechargeable lithium ion batteries. *Nano Lett.* 8, 2277–2282. doi: 10.1021/nl800957b

Yuan, C., Li, J., Hou, L., Zhang, X., Shen, L., and Lou, X. W. (2012). Ultrathin mesoporous $NiCo_2O_4$ nanosheets supported on ni foam as

advanced electrodes for supercapacitors. *Adv. Funct. Mater.* 22, 4592–4597. doi: 10.1002/adfm.201200994

Yuan, C., Wu, H. B., Xie, Y., and Lou, X. W. (2014). Mixed transition-metal oxides: design, synthesis, and energy-related applications. *Angew. Chem. Int. Ed.* 53, 1488–1504. doi: 10.1002/anie.201303971

Zhou, B., Li, C., Qi, N., Jiang, M., Wang, B., and Chen. Z. (2018). Pore structure of mesoporous silica (KIT-6) synthesized at different temperatures using positron as a nondestructive probe. *Appl. Surf. Sci.* 450, 31–37. doi: 10.1016/j.apsusc.2018.03.223

Conflict of Interest Statement: The authors declare that the research was conducted in the absence of any commercial or financial relationships that could be construed as a potential conflict of interest.

Copyright © 2019 Ren, Wu, Xing, Han, Li, Li, Cheng, Wu, Zou and Hu. This is an open-access article distributed under the terms of the Creative Commons Attribution License (CC BY). The use, distribution or reproduction in other forums is permitted, provided the original author(s) and the copyright owner(s) are credited and that the original publication in this journal is cited, in accordance with accepted academic practice. No use, distribution or reproduction is permitted which does not comply with these terms.